Crystal Structure at 1.8 Å Resolution of CDP-D-Glucose 4,6-Dehydratase from *Yersinia pseudotuberculosis*[†,‡]

Erik M. Vogan,*[,§,||] Cornelia Bellamacina,[§,⊥] Xuemei He,[#] Hung-wen Liu,[#] Dagmar Ringe,*[,§] and Gregory A. Petsko*[,§]

Departments of Biochemistry and Chemistry and Rosenstiel Basic Medical Sciences Research Center, Brandeis University, Waltham, Massachusetts 02454, and Division of Medicinal Chemistry, College of Pharmacy, and Department of Chemistry and Biochemistry, University of Texas, Austin, Texas 78712

Received August 28, 2003; Revised Manuscript Received January 15, 2004

ABSTRACT: CDP-D-glucose 4,6-dehydratase catalyzes the conversion of CDP-D-glucose to CDP-4-keto-6-deoxyglucose in an NAD^+-dependent manner. The product of this conversion is a building block for a variety of primary antigenic determinants in bacteria, possibly implicated directly in reactive arthritis. Here, we describe the solution of the high-resolution crystal structure of CDP-D-glucose 4,6-dehydratase from *Yersinia pseudotuberculosis* in the resting state. This structure represents the first CDP nucleotide utilizing dehydratase of the short-chain dehydrogenase/reductase (SDR) family to be determined, as well as the first tetrameric structure of the subfamily of SDR enzymes in which NAD^+ undergoes a full reaction cycle. On the basis of a comparison of this structure with structures of homologous enzymes, a chemical mechanism is proposed in which Tyr157 acts as the catalytic base, initiating hydride transfer by abstraction of the proton from the sugar 4′-hydroxyl. Concomitant with the removal of the proton from the 4′-hydroxyl oxygen, the sugar 4′-hydride is transferred to the B face of the NAD^+ cofactor, forming the reduced cofactor and a CDP-4-keto-D-glucose intermediate. A conserved Lys161 most likely acts to position the NAD^+ cofactor so that hydride transfer is favorable and/or to reduce the pK_a of Tyr157. Following substrate oxidation, we propose that Lys134, acting as a base, would abstract the 5′-hydrogen of CDP-4-keto-D-glucose, priming the intermediate for the spontaneous loss of water. Finally, the resulting $\Delta^{5,6}$-glucoseen intermediate would be reduced suprafacially by the cofactor, and reprotonation at C-5′ is likely mediated by Lys134.

CDP-D-glucose 4,6-dehydratase (E_{od}) catalyzes the NAD^+-dependent conversion of CDP-D-glucose to CDP-4-keto-6-deoxyglucose by means of an irreversible intramolecular oxidation/reduction (*1*−*3*). This enzyme, and its homologues, catalyze the first committed step in the synthesis of 6-deoxyhexoses, thus providing a common entry into the pathway for the generation of secondary metabolites found in antibiotics, glycoproteins, and the bacterial lipopolysaccharide layer (*4*−*7*).

The 3,6-dideoxyhexoses, which are primarily found in the lipopolysaccharide layer of Gram-negative bacteria, can be synthesized directly from the 6-deoxyhexoses (*8*−*11*). These sugars are important antigenic determinants and a primary source of serological specificity (*8*, *12*, *13*). Further, these immunologically active sugars have been implicated as the cause of certain persistent postinfection disease states (*14*).

The 4,6-dehydratases have been studied well, both biochemically (*15*, *16*) and, in some cases, structurally (*17*, *18*). The chemical mechanism for the biosynthesis of 4-keto-6-deoxyhexoses is believed to proceed through three steps, as delineated in Scheme 1 (adapted from ref *15*). First, the enzyme-bound NAD^+ abstracts the 4′-hydride from the substrate, generating a 4-ketohexose intermediate. This intermediate then undergoes dehydration across the C-5−C-6 bond, giving rise to the 4-keto-$\Delta^{5,6}$-glucoseen, which is then reduced at the C-6 position to yield the 4-keto-6-deoxyhexose product.

During this reaction, the reduced NADH cofactor remains bound to the enzyme, a feature distinguishing this class of enzymes from the broader family whose members catalyze half-reactions using NAD^+ as a cofactor (*6*, *15*, *19*). The smaller family of enzymes to which E_{od} belongs has been categorized as an extension of the short-chain dehydrogenase/reductase (SDR) family, and can be partially distinguished on the basis of primary sequence motifs GXXGXXG and YXXXK (*20*−*22*). Structures have been determined for several of the enzymes in this subfamily, including UDP-galactose 4-epimerase [from both *Escherichia coli* (*23*, *24*) and *Homo sapiens* (*25*)], GDP-mannose 4,6-dehydratase

[†] This work was supported by NIH Grant GM-32415 to G.A.P. and D.R. and NIH Grant GM-35906 to H.-w.L.

[‡] Coordinates for E_{od} have been deposited in the Protein Data Bank as entry 1RKX.

* To whom correspondence should be addressed: Departments of Biochemistry and Chemistry and Rosenstiel Basic Medical Sciences Research Center, Brandeis University, 415 South St., Waltham, MA 02454-9110. Phone: (781) 736-4905. Fax: (781) 736-2405. E-mail: petsko@brandeis.edu or ringe@brandeis.edu.

[§] Brandeis University.

[||] Current address: Laboratory of Molecular Medicine, Children's Hospital-Enders 673, 320 Longwood Ave., Boston, MA 02115. E-mail: vogan@crystal.harvard.edu.

[⊥] Current address: Chiron Corp., 4560 Horton St., M/S 4.4, Emeryville, CA 94608. E-mail: cornelia_bellamacina@chiron.com.

[#] University of Texas.

10.1021/bi035547f CCC: $27.50
Published on Web 02/27/2004

Scheme 1

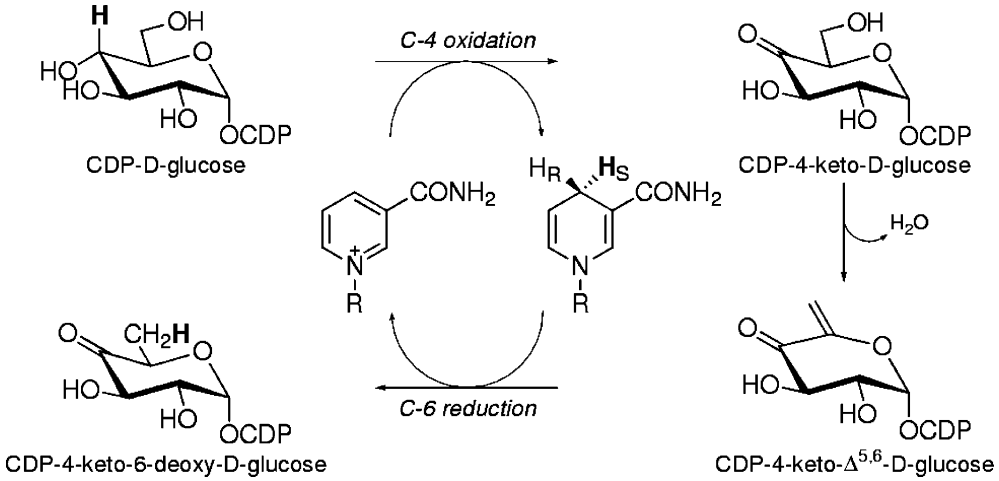

[from *E. coli* (*18*)], and TDP-glucose 4,6-dehydratase [from both *E. coli* and *Salmonella enterica* (*17*)]. Aside from the obvious differences in substrate specificity and activity, E_{od} distinguishes itself as the only enzyme of the subfamily that requires exogenous NAD^+ for full activity (*1*, *15*, *26*). Further, it is the only bacterial member of the subfamily known to occur in a tetrameric form, although another tetrameric member of this subfamily has been reported (*27*, *28*).

We report here the determination of the crystal structure of CDP-D-glucose 4,6-dehydratase from *Yersinia pseudotuberculosis* at 1.8 Å resolution. This structure represents the first CDP nucleotide utilizing dehydratase of the SDR family to be determined, as well as the first tetrameric structure for the subfamily of SDR enzymes which utilize NAD^+ as a catalytic prosthetic group. This structure allows us both to interpret more fully previous mutagenesis studies and to propose a detailed chemical mechanism for this enzyme.

EXPERIMENTAL PROCEDURES

Materials. CDP-glucose, NAD^+, and EDTA were purchased from Sigma. PEG 4000 was purchased from Fluka, and HEPES free acid was purchased from Research Organics. DEAE DE-52 resin was from Whatman, while an S200 HiPrep 16/60 gel filtration column was purchased from Pharmacia.

Expression and Purification of the Dehydratase. Expression and purification of recombinant *Y. pseudotuberculosis* dehydratase from *E. coli* have been described in detail (*27*, *29*). Briefly, the *Y. pseudotuberculosis* ascB gene was overexpressed in *E. coli* and then partially purified by ammonium sulfate precipitation at 65% saturation. This crude enzyme preparation was resuspended in purification buffer [100 mM KP_i and 1 mM EDTA (pH 7.5)], applied to a DEAE column, and then eluted with a linear gradient from 140 to 365 mM KP_i (pH 7.5). Samples containing significant enzyme activity were pooled and injected onto a HiPrep S200 gel filtration column equilibrated in purification buffer (*26*). The enzyme eluted from the gel filtration column at 160 kDa, the size expected for a tetramer. The pure enzyme was concentrated to 40 mg/mL (by Bradford) and flash-frozen in small aliquots using liquid nitrogen (*30*).

Crystallization and Data Collection. Crystals were grown by the hanging drop vapor diffusion method at 4 °C, as described previously (*27*). A frozen aliquot of purified enzyme at a concentration of 40 mg/mL was thawed, then mixed 1:1 with 5 mM NAD^+, and allowed to incubate for 15 min at 4 °C. Equal volumes of this enzyme/coenzyme solution were then mixed with precipitant solution [1.0 M ammonium sulfate, 2% (w:v) PEG 4000, and 100 mM K·HEPES (pH 7.5)]. The enzyme concentration was 0.25 mM under these conditions. After 2 days, these drops were microseeded with a 1×10^{-4} dilution of a crushed crystal from the previous generation. Crystals achieved maximum dimensions of 0.6 mm × 0.6 mm × 0.4 mm in ~2 weeks. These crystals had the symmetry of space group $P2_12_12_1$, with the following unit cell dimensions: $a = 99.9$ Å, $b = 115.9$ Å, and $c = 128.8$ Å. The asymmetric unit contained four monomers related by 222 noncrystallographic symmetry (*27*). For data collection, crystals were slowly transferred to an artificial mother liquor consisting of 1.4 M ammonium sulfate, 2% (w:v) PEG 4000, 25% (w:v) xylitol, and 100 mM K·HEPES (pH 7.5), and then the mixture was mounted on a cryoloop and plunged into liquid nitrogen.

A native X-ray data set was collected to 1.8 Å resolution at beamline X12B at the National Synchrotron Light Source (NSLS) [Brookhaven National Laboratory (BNL), Upton, NY]. The wavelength for this experiment was 1.0704 Å. Data were reduced with DENZO and scaled with SCALEPACK, both from the HKL package (*31*). Relevant X-ray data collection statistics are given in Table 1.

The first isomorphous heavy atom derivative was produced by incubating the enzyme/coenzyme solution, prepared as described above, with 1 molar equiv (0.25 mM) of ethylmercuric phosphate (EMP) for 15 min at 4 °C, prior to crystallization. The enzyme that reacted with higher concentrations of EMP failed to crystallize. Preparation of additional isomorphous heavy atom derivatives required the transfer of crystals to an artificial mother liquor consisting of 1.4 M lithium sulfate, 2% (w:v) PEG 4000, and 100 mM K·HEPES (pH 7.5) to avoid competing reactions with ammonia derived from the ammonium sulfate. Two additional isomorphous heavy atom derivatives could then be prepared by soaking with 0.1 mM potassium mercury iodide (PMTI) for 24 h or 0.5 mM potassium platinum nitrate (PN) for 36 h. The PMTI derivative data set, to 3.0 Å resolution,

Table 1: Crystallographic Data Collection Statistics[a]

	native	EMP	EMP MAD	PMTI	PN MAD
soak					
compound	−	$C_2H_5HgPO_4$	$C_2H_5HgPO_4$	$KHgI_4$	$K_2Pt(NO_2)_4$
concentration	−	1 molar equiv	1 molar equiv	0.1 mM	0.5 mM
time	−	15 min	15 min	24 h	36 h
beamline	NSLS X12B	NSLS X12B	NSLS X12C	NSLS X12B	APS BM14D
cell constants (Å)	99.90 (*a*), 115.87 (*b*), 126.83 (*c*)	99.73 (*a*), 115.74 (*b*), 127.24 (*c*)	99.88 (*a*), 115.84 (*b*), 127.38 (*c*)	99.88 (*a*), 116.09 (*b*), 127.38 (*c*)	99.81 (*a*), 116.40 (*b*), 126.86 (*c*)
mosaicity (deg)	0.5	0.5	0.3	1.1	0.6
wavelength (Å)	1.07040	1.00880	1.01024, 1.00493, 0.98600	1.00880	1.07258, 1.07189, 1.04629
resolution limit (Å)	36−1.8	40−3.0	50−2.4	40−3.0	85−2.5
completeness (%)	97.7 (93.4)	92.3 (93.8)	86.9 (44.9)	87.8 (69.7)	91.0 (62.7)
redundancy	5.8 (3.2)	6.4 (5.8)	3.1 (1.5)	6.2 (3.5)	7.8 (1.8)
R_{merge} (%)	6.6 (35.0)	4.6 (6.8)	5.6 (16.7)	5.7 (9.9)	7.9 (27.7)
I (error)	18.4 (2.6)	22.2 (16.0)	21.7 (6.3)	14.5 (7.4)	19.2 (3.8)
R_{iso} (%)	−	18.0 (20.9)	4.6 (11.3)	22.4 (27.1)	8.1 (33.5)
K_{emp}	−	9.0 (7.7)	1.4 (1.5)	10.7 (7.1)	2.5 (2.0)

[a] The EMP derivative was generated by reacting the enzyme with 1 molar equiv of EMP for 15 min prior to crystallization. Numbers in parentheses are statistics for the highest-resolution shell. For isomorphous derivatives, comparisons are between the native and derivative sets. For MAD data sets, comparisons are for inflection point data set vs remote data set. R_{merge} is defined as $\sum(|I - \langle I\rangle|)/\sum(I)$. R_{iso} is defined as $\sum(|F_{PH} - F_P|)/\sum(F_P)$, where F_{PH} is the derivative amplitude and F_P the native amplitude. K_{emp} is defined as $\sum(|F_{PH} - F_P|)/(0.5\sum(|D_{PH}|)$, where D_{PH} is the delta anomalous amplitude.

was collected using a wavelength of 1.0088 Å, at beamline X12B, BNL, NSLS. A three-wavelength (1.01024, 1.00493, and 0.98600 Å) multiwavelength anomalous diffraction (MAD) data set was collected for the EMP cocrystal derivative at beamline X12C, BNL, NSLS. A three-wavelength (1.07258, 1.07189, and 1.05629 Å) MAD data set for the PN derivative was collected at beamline BM14D of BioCARS [Advanced Photon Source (APS), Chicago, IL].

Each heavy atom derivative was scaled to the native data set using FHSCAL and SCALEIT, from the CCP4 program suite (*32*−*34*). The *R*-factor between the native enzyme and the PMTI derivative was 22.4%, to 3.0 Å resolution {$R = [\sum(|F_{PH} - F_P|)/\sum(F_P)] \times 100$, where F_P is the native structure factor and F_{PH} is the derivative structure factor}. *R*-factors between the rising edge anomalous data set and the remote data set for the EMP and PN derivatives were 4.6 and 8.1%, respectively.

Positions of the EMP and PN heavy atom binding sites were determined manually by inspection of anomalous difference Patterson maps calculated with peak anomalous X-ray data from 85 to 4.5 Å resolution. Four heavy atom binding sites were identified for the EMP derivative, while six heavy atom binding sites could be identified for the PN derivative. These derivatives were placed on a common origin by means of difference Fourier maps, which allowed the identification of four additional heavy atom binding sites in the EMP derivative data. Eight heavy atom binding sites in the PMTI derivative were determined from difference Fourier maps using combined phases from the EMP and PN derivatives. For each derivative, heavy atom binding positions and occupancies were refined using MLPHARE from the CCP4 package (*34*, *35*). This same program was used to generate Hendrickson−Lattman coefficients for each derivative, which were combined to yield the final experimental phase set (*36*). The overall figure of merit of that phase set was 0.52 from 85 to 2.5 Å resolution. This phase set was subjected to histogram matching, solvent flattening, and 4-fold noncrystallographic symmetry averaging using DM from the CCP4 suite, which yielded a phase set with a figure of merit of 0.71 (*34*, *37*−*39*).

Model Building and Structural Refinement. The density-modified, NCS-averaged electron density map was readily interpretable, and an initial model, consisting of 324 of the 357 amino acids for E_{od}, was built into this density using O (*40*). Density for the NAD^+ cofactor was unambiguous, and the cofactor was modeled into the initial averaged density. Both N- and C-termini were missing from this model, as were two stretches of residues (residues 202−227 and an entire loop from residue 290 to 300). CNS_SOLVE was used to refine this structure from a starting *R*-factor of 47.2% (R_{free} = 49.4%) (*41*, *42*). Several rounds of alternating refinement and manual rebuilding into $2F_o - F_c$ SIGMAA-weighted electron density maps brought the model to an *R*-factor of 22.9% (R_{free} = 26.6%) (*34*, *43*, *44*). Ice rings in the experimental diffraction data cause both the *R*-factor and R_{free} to be elevated in the resolution shells from 2.32 to 2.23 Å and from 1.93 to 1.87 Å. It was not possible to obtain frozen crystals without such ice rings, and it was also not possible to process the diffraction data to eliminate the ice rings without also eliminating the data in these shells. Refinement against the data to 1.80 Å, eliminating those two resolution shells, yields a more conventional *R*-factor of 21.4% (R_{free} = 24.1%). While the inclusion of the data to 1.8 Å does increase both the overall *R*-factor and R_{free}, it also significantly improves the appearance of the maps, so the structure is reported as refined against the full 1.8 Å resolution data set. The final model includes all residues except the N-terminal methionine and varying portions of the loop from residue 290 to 300, depending on the monomer. In addition, this model contains one NAD^+ moiety per monomer and 862 waters. This final model was evaluated with PROCHECK and is average or better in all statistical indicators of model quality when compared to a representative selection of well-refined structures at the same resolution (*34*, *45*). All residues fall within the allowed regions of a Ramachandran plot.

Modeling of the Substrate. The structures of both *E. coli* and human UDP-galactose 4-epimerase contain bound UDP-glucose (PDB entries 1XEL and 1EK5, respectively) (*24*, *25*). These two homologues of E_{od} were aligned to the final E_{od} model using the least-squares superposition tools within

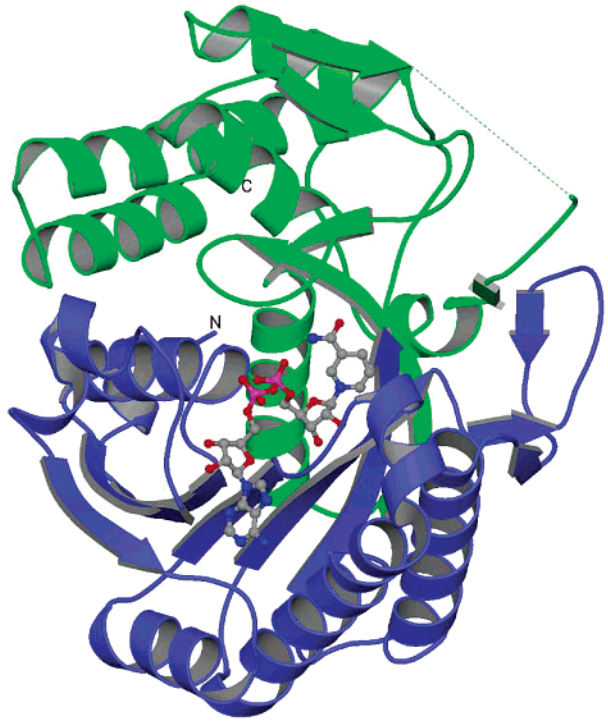

FIGURE 1: Ribbon diagram of the polypeptide chain fold of CDP-D-glucose 4,6-dehydratase from *Y. pseudotuberculosis*. The N-terminal cofactor binding domain is shown in blue, with the bound cofactor shown as a ball-and-stick model. The C-terminal substrate binding domain is colored green. The break in the connectivity for the substrate binding domain is shown as a dashed green line. The C-terminus is labeled just below its actual position, which would be obscured by a foreground helix. This figure was prepared with Molscript and Raster3D (*64*, *65*).

O (*40*). *E. coli* epimerase superimposed with an rmsd for Cα atoms of 1.7 Å over 274 atoms, while the human epimerase superimposed with an rmsd for Cα atoms of 1.8 Å over 275 atoms. More importantly, the NAD^+ cofactors (NAI inhibitor in the case of the human epimerase) were well aligned, with a distance of 0.41 Å to C-4 of E_{od} for the *E. coli* enzyme and 0.60 Å to C-4 of E_{od} for the human enzyme. UDP-glucose substrate molecules from these aligned epimerase structures were truncated at the oxygen joining the two phosphorus atoms of the substrate molecule, and the position of the glucose moiety was modeled into E_{od} and used to examine the active site residues.

RESULTS AND DISCUSSION

Tertiary and Quaternary Structure. The CDP-D-glucose 4,6-dehydratase monomer is roughly spherical and composed of two mixed α/β domains, as seen in Figure 1. The larger amino-terminal domain, composed of amino acids 1−193, binds the cofactor and consists of a central six-stranded parallel β-sheet, flanked by three α-helices to the outside of the molecule and one α-helix to the inside of the molecule. The longer of the two α-helices to the outside of this modified Rossman fold dinucleotide binding domain provides the largest of the structural elements involved in oligomer formation (*46*). The NAD^+ is positioned along the C-terminal end of the dinucleotide binding domain, facing the smaller carboxy-terminal domain, which is composed of amino acids 194−357. This substrate binding domain continues the final β-strand of the cofactor binding domain, and contributes a seventh strand to the central parallel β-sheet. This domain would, by analogy to other structures of this fold, position the substrate with the glucose in the proximity of the chemically active C-4 of the nicotinamide ring of the cofactor (*17*, *23*). The remainder of the substrate binding domain is composed of three long loops, three short β-strands, and five α-helices. One of those helices nestles parallel against the backside of the central β-sheet, with the other four helices running perpendicular to the central sheet (Figure 1). The substrate binding domain also contains a short, extended, β-like disordered region, of 5−10 residues, depending on the monomer, which presumably forms the distal side of the substrate binding pocket. The lack of order in part of this domain is most likely due to the absence of substrate (or substrate analogue) under crystallization conditions.

The complete enzyme tetramer is shown in Figure 2, with the individual monomers labeled A−D. After refinement, the tetramer exhibited near-exact 222 symmetry, with the largest deviation from 180° (an exact 2-fold rotation) being 0.4°. A four-helix bundle, formed from the two long helices of each monomer, provides the primary stabilizing force for the AB dimer. These helices are inserted into a loop of the dinucleotide binding domain. The AB and CD dimer local 2-fold rotation axes are parallel to the crystallographic *x* axis and thus are responsible for the pseudo-origin peak seen on the native self-Patterson map (*27*). The AD dimer interface is formed from two partially structured loops and a two-turn α-helix, as well as a half-dozen waters conserved among all monomers. One of these loops is contributed by the dinucleotide binding domain and occurs in the same insert as one of the helices that forms the four-helix bundle. The other loop and the two-turn helix are contributed by the substrate binding domain. Although the two sets of dimer interactions occur through very different sets of secondary structure elements, the amount of surface area buried by these interactions is not significantly different. The four-helix bundle, comprising a helix from residue 108 to 122 and another helix from residue 155 to 173, buries approximately 2280 $Å^2$, or ∼16% of the surface area of the enzyme monomer. The loops that form the AD dimer interface, defined as residues 140−149, 262−273, and 299−311, bury approximately 1750 $Å^2$, or ∼12% of the surface area of the enzyme monomer. The surface area buried by the latter region is most likely underestimated, as that buried area is likely to include at least a portion of the disordered loop region. A lack of order in that region of the crystal structure might, however, argue against any significant additional stabilization. It should be noted that the buried surface calculations are quite crude, and as a result, these numbers should be viewed as gross approximations. All buried surface calculations were performed with ASC (*47*, *48*).

When SDR subfamily enzyme structures are aligned (sequence alignment shown in Figure 6), the most striking feature is the absolute conservation of the two long helices on the backside of the central parallel β-sheet. Those helices, when mated after a local 2-fold symmetry operation, form the four-helix bundle dimerization domain which stabilizes the AB dimer in E_{od}. This result agrees with evidence that all members of this subfamily of enzymes form obligate homodimers, primarily through interactions in these conserved helices (*22*). It is also likely that any monomer crosstalk or asymmetry in the dimer, specifically anticoop-

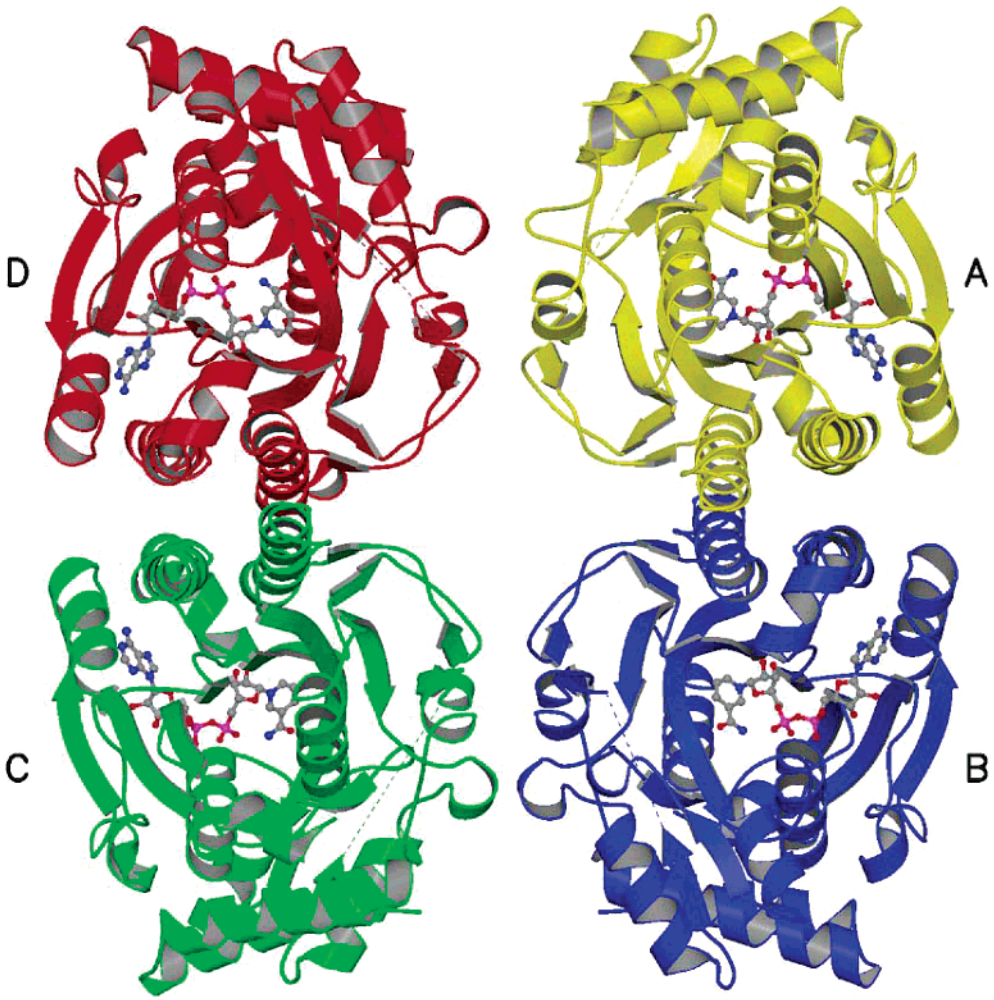

FIGURE 2: Quaternary association of enzyme monomers of E_{od}, as observed in the crystal. Individual monomers are shown in different colors and are also referenced by letter (A−D). The bound NAD^+ cofactor is shown in ball-and-stick form. This figure was prepared with Molscript and Raster3D (*64*, *65*).

erativity in binding cofactor, would be brought about by changes in the interactions between these helices (*15*). This conclusion is supported by reports in the literature that if dissociated to monomers, enzymes of this subfamily only re-form dimers in the presence of the NAD^+ cofactor (*9*, *26*, *49*). The requirement that a cofactor be bound for dimer formation to occur seems to hint at a general mechanism of monomer crosstalk, which likely has consequences beyond the formation of a higher-order oligomeric state.

Dinucleotide Binding Site. A schematic representation of the NAD^+ cofactor binding site appears in Figure 3. The majority of the cofactor binding interactions are hydrophobic, with a large number of those interactions serving to anchor the adenine nucleotide portion of the cofactor in a hydrophobic cleft. This observation is in good agreement with the general features of the adenine binding pocket originally described by Rossman et al. (*46*). This agreement abates upon examination of the number of hydrogen bonds made to the adenine moiety. In glyceraldehyde-3-phosphate dehydrogenase, representative of the dehydrogenase family, only two hydrogen bonds are formed to the adenine moiety, both to atom AO2*, presumably serving to orient the adenine ring system correctly in the binding cleft. In contrast, E_{od} makes five hydrogen bonds to the adenine nucleotide, one to each cofactor atom capable of participating in hydrogen bond

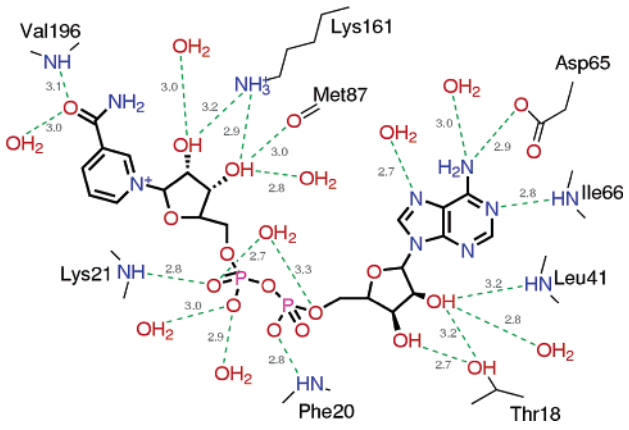

FIGURE 3: Schematic representation of the interactions involved in the binding of NAD^+. Hydrogen bonds between the bound cofactor and the protein are shown as dashed lines with the lengths specified in angstroms.

formation (Figure 3). This network of hydrogen bonds likely serves not only to orient the cofactor but also to significantly stabilize cofactor binding. The modified phosphate binding consensus sequence GXXGXXG allows the first two glycines to participate in hydrophobic interactions with the adenine nucleotide. These glycines also permit a tight turn into α-helix αB, the amino terminus of which is positioned such

that the positive helix dipole neutralizes some portion of the cofactor phosphate oxygen negative charge (*50*). In addition, the backbone nitrogen atoms of the final two X residues in the GXXGXXG motif, Phe20 and Lys21, are positioned to make hydrogen bonds with the cofactor phosphate oxygens, further neutralizing this source of negative charge and anchoring the cofactor. The number of hydrophobic interactions with the nicotinamide nucleotide are reduced when compared to the number with the adenine moiety, suggesting this portion of the cofactor might be more mobile. Solvent accessibility calculations lend weight to this argument, indicating that the reactive position of the nicotinamide moiety is quite open to solvent. Several hydrogen bonds are made to the ribosyl group and carboxamide oxygen of the nicotinamide nucleotide, serving to orient the reactive carbon. Lysine 161 makes hydrogen bonds to both nicotinamide ribosyl hydroxyl oxygens and is absolutely conserved throughout the dehydratase family. This observation suggests a common role for this residue in steering the reactive position of the cofactor into the proximity of the substrate and possibly in enhancing the reactivity of the nicotinamide group (*66*). In support of this idea is the report that mutation of the equivalent lysine in the UDP-galactose 4-epimerase decreases the activity of that enzyme by 3 orders of magnitude (*51*).

Comparison with UDP-Galactose 4-Epimerase. The UDP-galactose 4-epimerase from *E. coli* has been studied extensively, both biochemically and structurally (*7*, *23*−*25*, *52*−*55*). The epimerase was chosen for comparison in an attempt to understand the functioning of the active site of E_{od}. This structural comparison must be made in the context of the mechanistic differences between the two enzymes, to obtain a clear understanding of the meaning of any conserved (or nonconserved) residues. In addition, the epimerase and the dehydratase come from two very different species of Enterobacteriaceae, meaning that any side chain differences must also be examined through the lens of evolutionary divergence (*56*).

The epimerase catalyzes the interconversion of UDP-glucose and UDP-galactose by the removal and then replacement, in a nonstereospecific manner, of the hydride found at C-4′ of the hexose (*6*, *19*, *23*). This transient oxidation/reduction reaction utilizes a bound NAD^+ cofactor and bears a striking resemblance to the reaction carried out by E_{od}, with some important exceptions (*7*). The hydride transferred by the epimerase returns to the same carbon from which it was originally taken, albeit in a different stereochemical orientation (*6*). In contrast, E_{od} returns the hydride taken from C-4′ of the hexose sugar to the methyl group formed at C-6′ after the elimination of water (*26*). It is therefore expected that the epimerase active site will contain all of the molecular machinery necessary for abstraction of the hydrogen from the hexose 4′-hydroxyl, leading to transfer of 4′-hydride to the cofactor. But the epimerase would be expected to lack any machinery for abstracting the hydrogen from C-5′, leading to the elimination of water from C-6′. In addition, the NAD^+ cofactor is not free to dissociate from the epimerase between reaction cycles, as is the case with E_{od}, leading to the expectation that the cofactor would be either more deeply buried or more tightly bound in the epimerase structure (*23*).

FIGURE 4: Structural alignment of CDP-D-glucose 4,6-dehydratase (blue) and UDP-D-galactose 4-epimerase (green). Conserved secondary structure elements are shown in a ribbon representation, while nonconserved stretches are shown in a coil representation. This figure was prepared with Molscript and Raster3D (*64*, *65*).

An epimerase structure with a bound NADH cofactor and UDP-glucose ligand (PDB entry 1XEL) was chosen for this comparison (*24*, *57*). Least-squares superposition of that epimerase structure with the E_{od} structure aligns 271 of 338 α-carbon positions, or 80% of the epimerase model, with an overall root-mean-square deviation of 1.7 Å. The aligned structures are shown in Figure 4. The cofactor binding domain shows greater structural conservation, defined as a stretch of three or more residues with an rmsd for Cα atoms of <6 Å, than does the substrate binding domain, with differences between only 33 of 200 amino acids, or 16% of the residues that form this domain. In contrast, the smaller carboxy-terminal domain shows differences between 34 of 138 amino acids, or 25% of the residues that form the substrate binding domain. The cofactor is bound in the same extended conformation in both enzymes and superimposes clearly, with an rmsd of 0.8 Å for all cofactor atoms after structural alignment based solely on protein α-carbon positions. The fact that the stereochemical preference of the hydride transfer to and from NAD^+ was determined to be *pro-S* for both enzymes (*58*, *59*) is consistent with the highly homologous cofactor binding domain in these enzymes. A similar stereochemical outcome (*60*) and structural homology (*61*) had also been reported for L-myoinositol-1-phosphate synthase, which catalyzes the isomerization of glucose 6-phosphate to L-myoinositol 1-phosphate. All of these enzymes share three common features; they use NAD^+ catalytically, act on sugar substrates, and are "*si* face" specific with respect to the transfer of one of the diastereotopic

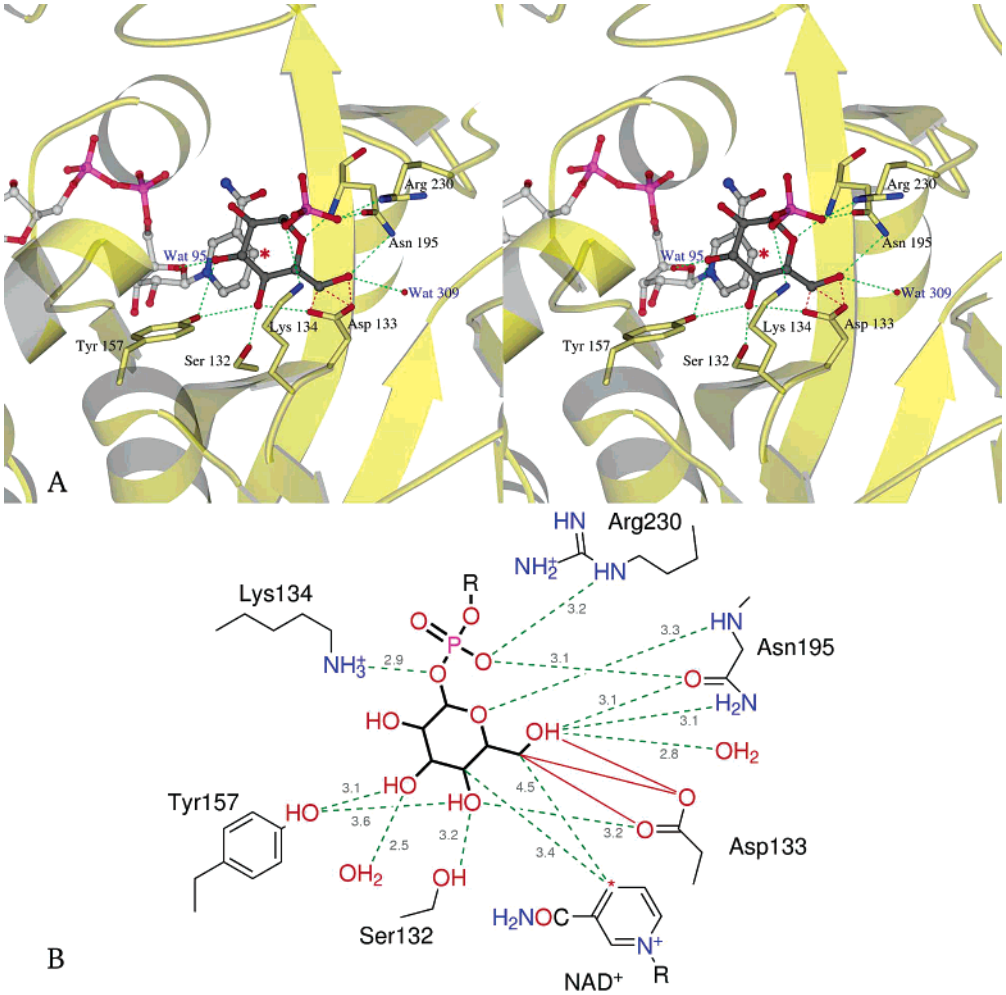

FIGURE 5: (A) Stereoview representation of possible interactions between the modeled glucose moiety of the CDP-D-glucose substrate of E_{od} and the active site residues. (B) Schematic representation of the same interactions, providing distances between key atoms. The substrate position is based on the known mode of binding of sugar substrates to other members of the family of enzymes to which E_{od} belongs, with superposition of their structures with that of E_{od} as shown in Figure 4. Interactions are depicted as in Figure 3. Close contacts are shown as red solid lines; these would presumably be relieved by small conformational changes in the actual enzyme−substrate complex. The cofactor reactive carbon has been marked with a red asterisk. The stereoview was prepared with Molscript (*64*).

methylene hydrogens at C-4 of the nicotinamide nucleotide coenzyme. It is possible that these enzymes have evolved from a common progenitor whose catalytic core has persevered throughout the enzyme's subsequent diversification.

The high degree of similarity found in the cofactor binding domain led to the expectation that useful information could be gained from an examination of the UDP-glucose ligand bound in the epimerase structure. The examination and comparison to the structure of E_{od} will be limited to the glucose moiety of the ligand, as other interactions in the dehydratase structure are either absent or disrupted as a result of the disorder in the substrate binding domain. A diagram of the residues involved in glucose interactions in E_{od}, based on this model, is shown in Figure 5.

In the epimerase, it has been proposed that residues Tyr149 (a part of the SDR fingerprint region) and Ser124, acting together, are likely the general acid−base catalyst needed to initiate hydride transfer to the NAD^+ cofactor (*24*). Site-directed mutagenesis studies lend considerable weight to that argument, suggesting that Tyr149 and Ser124 might act together as a proton couple, with Tyr149 being the ultimate proton acceptor (*53*, *54*). In the epimerase structure, Asn179, Asn199, and Tyr299 are thought to act as anchors, helping to stabilize the ligand in a productive conformation (*24*). Asn179 and Tyr299 form hydrogen bonds to the sugar 6′-hydroxyl group, while Asn199 forms a hydrogen bond to the sugar 2′-hydroxyl.

A comparison with the E_{od} structure finds equivalents for most of these residues. Ser124 and Tyr149 in the epimerase structure superimpose directly onto Ser132 and Tyr157, respectively, in E_{od}. Epimerase residue Asn179, which forms a hydrogen bond with both the sugar 6′-hydroxyl and a substrate phosphate oxygen, superimposes directly onto E_{od} residue Asn195, which would be capable of making the same interactions. It is at this point that the similarities begin to disappear. Epimerase residue Asn199 occupies the same space as does E_{od} residue Arg206. While Arg206 of E_{od} might form a hydrogen bond that is necessary for substrate orientation, it is more likely that this residue interacts with substrate bridging phosphate oxygen atoms and has simply occupied this position in the absence of substrate. There is no E_{od} residue in the vicinity of epimerase residue Tyr299, which is thought to anchor the substrate 6′-hydroxyl group. E_{od} residue Asp133 does approach the substrate 6′-hydroxyl group from the opposite side, and might play a functionally equivalent role in substrate orientation. E_{od} has one residue,

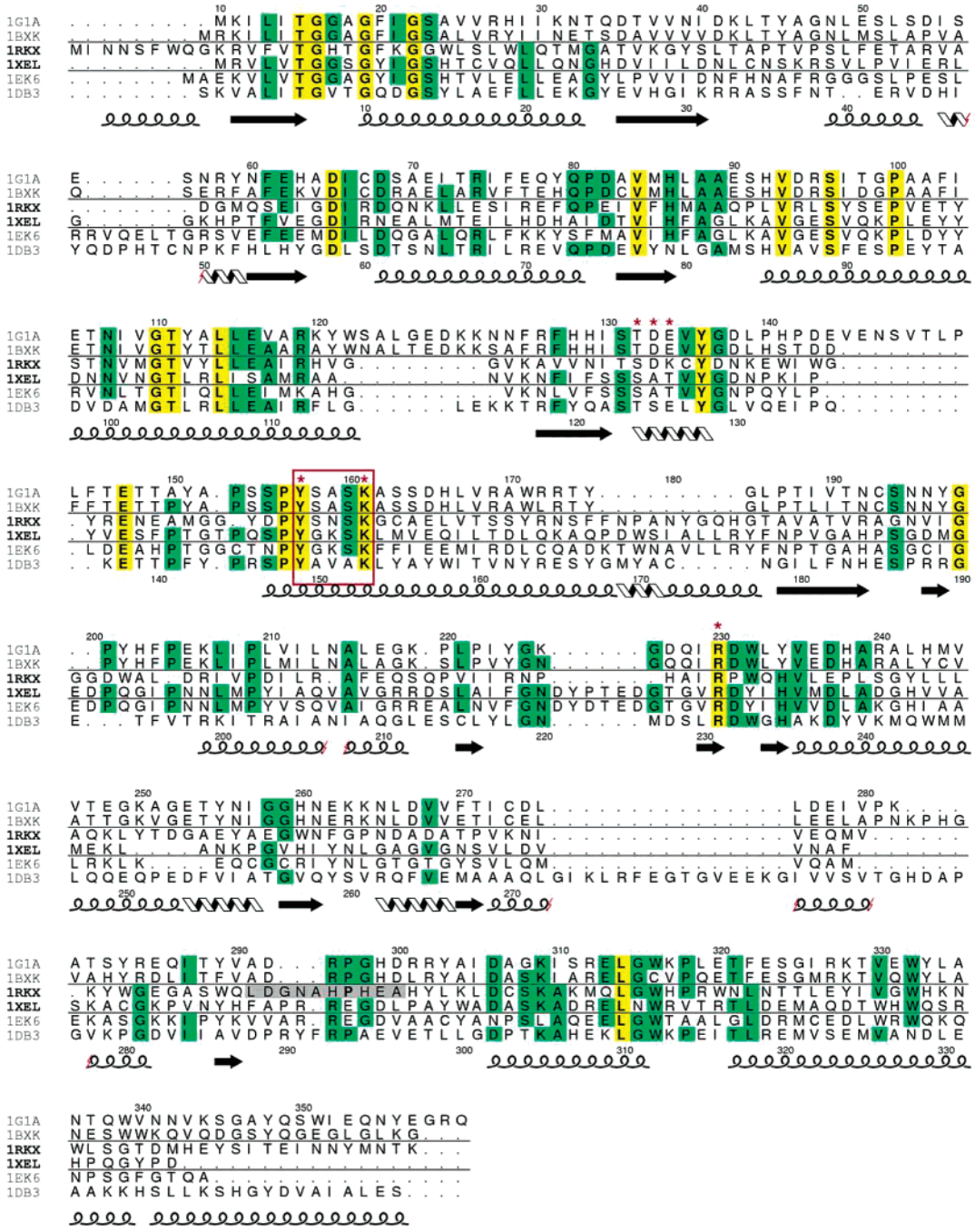

FIGURE 6: Sequence alignment of some dehydratase family members. The E_{od} sequence numbering is given at the top of the alignment, and the *E. coli* epimerase numbering is given above the secondary structure representation. Residues disordered in the E_{od} structure appear on a gray background. Residues conserved in all sequences appear on a yellow background, while residues conserved in four or more sequences appear on a green background. Active site residues are marked with a red asterisk, and the SDR signature sequence (YXXXK) is marked with a red box. Secondary structure is shown for E_{od}, with β-strands represented as arrows, α-helices as rounded helices, and 3/10-helices as diagonal helices. Sequences are identified by their PDB entry: 1G1A for *S. enterica* Dtdp-glucose 4,6-dehydratase, 1BXK for *E. coli* Dtdp-glucose 4,6-dehydratase, 1RKX for E_{od}, 1XEL for *E. coli* UDP-galactose 4-epimerase, 1EK6 for *H. sapiens* UDP-galactose 4-epimerase, and 1DB3 for *E. coli* GDP-mannose 4,6-dehydratase. This figure was prepared with Alscript (*67*).

Lys134, for which there is no equivalent in the epimerase structure. That residue occupies an extended conformation, with the terminal amino group positioned below the substrate 5′-carbon.

This comparison was repeated with a structure of the human UDP-galactose 4-epimerase with the bound NADH cofactor and UDP-glucose ligand (PDB entry 1EK6), to verify alignment of the functionally important side chains (*25*). Least-squares superposition of the human epimerase structure with the E_{od} structure aligns 275 of 346 α-carbon positions, again 80% of that model, with an overall root-mean-square deviation of 1.9 Å. The residue equivalencies from the human enzyme to the *E. coli* enzyme are as follows: Ser132 maps to Ser124, Tyr157 to Tyr149, Asn187 to Asn179, Asn207 to Asn199, and Met307 to Tyr299. When the human enzyme is aligned with E_{od} in this way, with the exception of Met307, side chains from the human epimerase overlap almost exactly with the side chains examined in the *E. coli* epimerase. This comparison suggests that while Tyr299 from the *E. coli* structure may act to stabilize the

Scheme 2

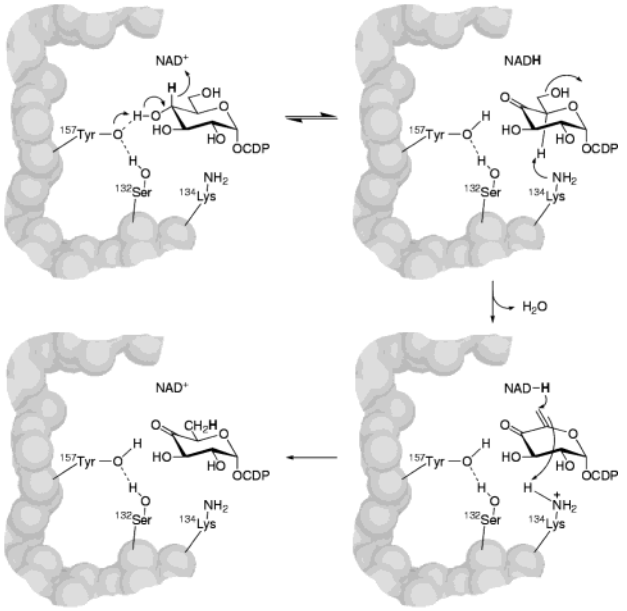

substrate, stabilization is not necessary for the epimerization reaction to proceed. There are no equivalents for E_{od} residues Asp133 and Lys134 found in the human epimerase structure.

It must be noted that these comparisons are model studies, based on the position of the UDP-glucose substrate in the structurally aligned epimerase structures. It is readily apparent that this method of positioning the ligand gives low-quality results as residue Asp133 from the E_{od} structure makes an unreasonably close approach to the modeled substrate sugar moiety. Still, after alignment of either epimerase structure with E_{od}, distances from E_{od} side chains to the glucose moiety atoms of either epimerase ligand differ by less than 0.1 Å, suggesting that there is enough structural fidelity that meaningful information can be extracted, and that the model exercise is useful in that it allows a possible chemical mechanism to be proposed.

Proposed Chemical Mechanism. The chemical reaction mechanism shown in Scheme 2 is proposed on the basis of the structure comparison with UDP-galactose 4-epimerase (residue numbers are those for E_{od}). In this scheme, Tyr157 would act as the catalytic base, which initiates hydride transfer by abstraction of the proton from the sugar 4′-hydroxyl. The pK_a of this tyrosine may be lowered by electostatic stabilization of the phenolate anion by the neighboring conserved Lys161 residue. Another possibility involves Ser132 and Tyr157 acting in concert as a proton shuttle, as proposed originally for the UDP-galactose 4-epimerase, or the tyrosine might act alone as the base with the serine residue acting to modulate the tyrosine pK_a by hydrogen bonding (*54*). Given the rather high pK_a of the serine and the proximity of the tyrosine phenolic oxygen to both the sugar 4′-hydroxyl and the side chain of Lys161, Tyr157 is depicted as the active site base in the reaction scheme, although there is no evidence in the specific case of E_{od} at present to support this choice over Tyr157 acting in concert with Ser132 as the proton shuttle. Concomitant with the removal of the proton from the 4′-hydroxyl oxygen, the sugar 4′-hydride would be transferred to the B face of the NAD^+ cofactor, resulting in a reduced cofactor and the CDP-4-keto-D-glucose intermediate. Although the conserved Lys161 is not depicted explicitly in the reaction scheme, it most likely acts to position the NAD^+ cofactor so that hydride transfer is favorable and/or to reduce the pK_a of Tyr157. It has been observed that mutation of the equivalent lysine in UDP-galactose 4-epimerase (epimerase Lys153) severely reduces the level of reductive inhibition of the cofactor, suggesting that this lysine might also play a role in increasing the reactivity of the bound NAD^+ cofactor (*51*). Lys161 is positioned near Tyr157, and there is precedent for a role for lysine in proton transfer in such reactions. In kinetic and structural studies of the unrelated NADP-dependent oxidoreductase human aldose reductase, Lys77 appears to mediate proton transfer from Tyr48 to the substrate during aldehyde reduction (*62*).

The remainder of the proposed mechanism is unique to E_{od}. Following substrate oxidation, it is proposed that residue Lys134, acting as a base, would abstract the 5′-hydrogen of CDP-4-keto-D-glucose, priming the intermediate for the spontaneous loss of water. Lysine 134 is in the proximity of C-5′, at a distance of only 3 Å, and is the only residue with the correct stereochemical orientation to abstract the 5′-proton from the CDP-4-keto-D-glucose intermediate. Although Lys134 has the correct stereochemical orientation and proximity to act as a catalytic base, there is no apparent means of lowering its pK_a. In addition, the group that ultimately acts as an acid, donating a proton to the leaving 6′-hydroxyl group, is not apparent. The solvent might act as the ultimate hydrogen donor for this hydroxyl, either as a bulk solvent or as a specific water molecule hydrogen bonded to a residue like Asp133. As an alternative, Asp133 might act through either strain or electrostatic repulsion to make the 6′-hydroxyl a more favorable leaving group. The water elimination step is the crystallographically least well-defined portion of the reaction mechanism, and all comments on this step are highly speculative. Finally, the $\Delta^{5,6}$-glucoseen intermediate would be reduced by the cofactor, and the 5′-hydrogen from Lys134 would be replaced. The cofactor is positioned for suprafacial hydride return, as expected from the isotope exchange experiments (*26*). Unfortunately, the NAD^+ cofactor is simply too far away from C-6′ in the model studies, suggesting that some small movement of either the intermediate or cofactor would be necessary to complete the reaction cycle.

The return of the 5′-hydrogen by Lys134 is in good agreement with solvent isotope exchange experiments. Any hydrogen associated with Lys134 would be expected to exchange quickly with solvent, accounting for the incorporation of deuterium at the 5′-position when the enzymatic reaction is carried out in a deuterated solvent (*6*, *49*). If the proposed active site residues of E_{od} are mapped to the structures of the *E. coli* or *S. enterica* TDP-glucose 4,6-dehydratase by least-squares alignment, side chain identity and spatial positioning are largely conserved (*17*, *63*). While the nature of the presumed serine−tyrosine shuttle remains little changed in those enzymes (the serine is replaced with a threonine in the *S. enterica* structure), both TDP dehydratases place a glutamate in the position occupied by Lys134 in E_{od}. The presence of those functional groups, capable of acting as a general base, in enzymes expected to carry out similar reactions is thus in good agreement with the assignment of Lys134 as an active site base in E_{od}.

The fate of the 4′-hydroxyl proton transferred to Tyr157 at the beginning of the reaction cycle is left undetermined in the proposed mechanism. While it is possible to presume that this hydrogen is carried away in bulk solvent, it is likely that nature has employed a more elegant means of returning the enzyme to the ground state. Insight into such a return mechanism, if one exists, will undoubtedly require additional detailed structural studies of this enzyme with a bound substrate or substrate analogues.

ACKNOWLEDGMENT

We thank Anthony Morollo, Brian Bahnson, and James Clifton for data collection assistance and helpful discussions.

REFERENCES

1. Matsuhashi, S., Matsuhashi, M., Brown, J. G., and Strominger, J. L. (1966) Enzymatic synthesis of cytidine diphosphate 3,6-dideoxyhexoses: III. Cytidine diphosphate D-glucose oxidoreductase, *J. Biol. Chem. 241*, 4283−4287.
2. Bevill, R. D. (1968) The mechanism of action of CDP-glucose oxidoreductase, *Biochem. Biophys. Res. Commun. 30*, 595−599.
3. He, X., and Liu, H.-w. (2002) Mechanism of enzymatic C−O bond cleavage in deoxyhexose biosynthesis, *Curr. Opin. Chem. Biol. 6*, 590−597.
4. Matsuhashi, S., Matsuhashi, M., Brown, J. G., and Strominger, J. L. (1964) Enzymatic synthesis of cytidine diphosphate ascarylose, *Biochem. Biophys. Res. Commun. 15*, 60−64.
5. Elbein, A. D., and Heath, E. C. (1965) The biosynthesis of cell wall lipopolysaccharide in *Escherichia coli*: II. Guanosine diphosphate 4-keto-6-deoxy-D-mannose, an intermediate in the biosynthesis of guanosine diphosphate colitose, *J. Biol. Chem. 240*, 1926−1931.
6. Walsh, C. (1979) *Enzymatic Reaction Mechanisms*, W. H. Freeman and Co., New York.
7. Gabriel, O., and Van Lenten, L. (1978) The interconversion of monosaccharides, in *The biochemistry of carbohydrates II* (Manners, D. J., Ed.) Vol. 16, pp 1−36, University Park Press, Baltimore.
8. Makela, P. H., and Stocker, B. A. D. (1984) Genetics of lipopolysaccharide, in *Handbook of endotoxin* (Rietschiel, E. Th., Ed.) Vol. 1, pp 59−137, Elsevier, New York.
9. Matsuhashi, S., Matsuhashi, M., and Strominger, J. L. (1966) Enzymatic synthesis of cytidine diphosphate 3,6-dideoxyhexoses: I. Over-all reactions, *J. Biol. Chem. 241*, 4267−4274.
10. Thorson, J. S., Lo, S. F., Ploux, O., He, X., and Liu, H.-w. (1994) Studies of the biosynthesis of 3,6-dideoxyhexoses: molecular cloning and characterization of the *asc* (ascarylose) region from *Yersinia pseudotuberculosis* serogroup VA, *J. Bacteriol. 176*, 5483−5493.
11. He, X., and Liu, H.-w. (2002) Formation of unusual sugar: mechanistic studies and biosynthetic applications, *Annu. Rev. Biochem. 71*, 701−754.
12. Verma, N. K., Quigley, N. B., and Reeves, P. R. (1988) O-Antigen variation in *Salmonella* spp.: *rfb* gene clusters of three strains, *J. Bacteriol. 170*, 103−107.
13. Liu, D., Verma, N. K., Romana, L. K., and Reeves, P. R. (1991) Relationship among the *rfb* Regions of *Salmonella* Serovars A, B and D, *J. Bacteriol. 173*, 4814−4819.
14. Granfors, K., Merilahti-Palo, R., Luukkainen, R., Mottonen, T., Lahesmaa, R., Probst, P., Marker-Hermann, E., and Toivanen, P. (1998) Persistence of *Yersinia* antigens in peripheral blood cells from patients with Yersinia enterocolitica O:3 infection with or without reactive arthritis, *Arthritis Rheum. 41*, 855−862.
15. He, X., Thorson, J. S., and Liu, H.-w. (1996) Probing the coenzyme and substrate binding events of CDP-D-glucose 4,6-dehydratase: mechanistic implications, *Biochemistry 35*, 4721−4731.
16. Hegeman, A. D., Gross, J. W., and Frey, P. A. (2001) Probing catalysis by *Escherichia coli* dTDP-glucose 4,6-dehydratase: identification and preliminary characterization of functional amino acid residues at the active site, *Biochemistry 40*, 6598−6610.
17. Allard, T. M., Giraud, M.-F., Whitfield, C., Graninger, M., Messner, P., and Naismith, J. H. (2001) The crystal structure of dTDP-D-glucose 4,6-dehydratase (RmIB) from *Salmonella enterica* serovar *typhimurium*, the second enzyme in the dTDP-L-rhamnose pathway, *J. Mol. Biol. 307*, 283−295.
18. Somoza, J. R., Menon, S., Schmidt, H., Joseph-McCarthy, J., Dessen, A., Stahl, M. L., Somers, W. S., and Sullivan, F. X. (2000) Structural and kinetic analysis of *Escherichia coli* GDP-mannose 4,6-dehydratase provides insights into the enzyme's catalytic mechanism and regulation by GDP-fucose, *Structure 8*, 123−135.
19. Frey, P. A. (1987) Complex pyridine nucleotide-dependent transformations, in *Pyridine Nucleotide Coenzymes* (Dolphin, D., Poulson, R., and Avramovic, O., Eds.) Part B, pp 461−511, Wiley-Interscience, New York.
20. Baker, M. E., and Blasco, R. (1992) Expansion of the mammalian 3-β-hydroxysteroid dehydrogenase/plant dihydroflavonol reductase superfamily to include bacterial cholesterol dehydrogenase, a bacterial UDP-galactose 4-epimerase, and open reading frames in vaccinia virus and fish lyphocystis disease virus, *FEBS Lett. 301*, 89−93.
21. Holm, L., Sanders, C., and Murzin, A. (1994) Three sisters, different names, *Nat. Struct. Biol. 1*, 146−147.
22. Jornvall, H., Persson, B., Krook, M., Atrian, S., Gonzalez-Duarte, R., Jeffery, J., and Ghosh, D. (1995) Short-chain dehydrogenases/reductases (SDR), *Biochemistry 34*, 6003−6013.
23. Bauer, A. J., Rayment, I., Frey, P. A., and Holden, H. M. (1992) The molecular structure of UDP-galactose 4-epimerase from *Escherichia coli* determined to 2.5 Å resolution, *Proteins: Struct., Funct., Genet. 12*, 372−381.
24. Thoden, J. B., Frey, P. A., and Holden, H. M. (1996) Molecular structure of the NADH/UDP-glucose abortive complex of UDP-galactose 4-epimerase from *Escherichia coli*: implications for the catalytic mechanism, *Biochemistry 35*, 5137−5144.
25. Thoden, J. B., Wohlers, T. M., Fridovich-Keil, J. L., and Holden, H. M. (2000) Crystallographic evidence for Try 157 functioning as the active site base in human UDP-galactose 4-epimerase, *Biochemistry 39*, 5691−5701.
26. Yu, Y., Russell, R. N., Thorson, J. S., Liu, L.-d., and Liu, H.-w. (1992) Mechanistic studies of the biosythesis of 3,6-dideoxyhexoses in *Yersinia pseudotuberculosis*, *J. Biol. Chem. 267*, 5868−5875.
27. Vogan, E. M., Bellamacina, C. R., He, X., Foxman, B. M., Ringe, D., Liu, H.-w., and Petsko, G. A. (2002) Purification, crystallization, and molecular symmetry of CDP-D-glucose 4,6-dehydratase from *Yersinia pseudotuberculosis*, *Acta Crystallogr. D58*, 370−373.
28. Mulichak, A. M., Bonin, C. P., Reiter, W.-d., and Garavito, R. M. (2002) Structure of the MUR1 GDP-mannose 4,6-dehydratase from *Arabidopsis thaliana*: Implications for ligand binding and specificity, *Biochemistry 41*, 15578−15589.
29. Vogan, E. M. (2000) The X-ray Crystal Structure of CDP-D-glucose 4,6-dehydratase from Yersinia pseudotuberculosis, Ph.D. Thesis, Brandeis University, Brandeis, MA.
30. Bradford, M. M. (1976) A Rapid and Sensitive Method for the Quantitation of Microgram Quantities of Protein Utilizing the Principle of Protein-Dye Binding, *Anal. Biochem. 72*, 248−254.
31. Otwinowski, Z., and Minor, W. (1997) Processing of X-ray diffraction data collected in oscillation mode, in *Methods in Enzymology* (Carter, C. W., Jr., and Sweet, R. M., Eds.) Vol. 276, pp 307−326, Academic Press, New York.
32. Kraut, J., Sieker, L. C., High, D. F., and Freer, S. T. (1962) Chymotrypsinogen: a three-dimensional Fourier synthesis at 5 Å resolution, *Proc. Natl. Acad. Sci. U.S.A. 48*, 1417−1424.
33. Howell, P. L., and Smith, G. D. (1992) Identification of heavy-atom derivatives by normal probability methods, *J. Appl. Crystallogr. 25*, 81−86.
34. Collaborative Computational Project, Number 4 (1994) The CCP4 Suite: Programs for Protein Crystallography, *Acta Crystallogr. D50*, 760−763.
35. Otwinowski, Z. (1991) in *Isomorphous Replacement and Anomalous Scattering* (Wolf, W., Evans, P. R., and Leslie, A. G. W., Eds.) SERC Daresbury Laboratory, Warrington, U.K.
36. Hendrickson, W. A., and Lattman, E. E. (1969) Representation of phase probability distributions for simplified combination of independent phase information, *Acta Crystallogr. B26*, 136−143.
37. Wang, B. C. (1985) Resolution of the phase ambiguity in macromolecular crystallography, in *Methods in Enzymology* (Wycoff, H. W., Hirs, C. H. W., and Timasheff, S. N., Eds.) Vol. 115, pp 90−112, Academic Press, New York.

38. Cowtan, K. D., and Main, P. (1993) Improvement of macromolecular electron-density maps by the simultaneous application of real and reciprocal space constraints, *Acta Crystallogr. D49*, 148−157.
39. Cowtan, K. D., and Main, P. (1998) Miscellaneous algorithms for density modification, *Acta Crystallogr. D54*, 487−493.
40. Jones, T. A., Zou, J.-Y., Cowan, S. W., and Kjeldgaard, M. (1991) Improved methods for building protein models in electron density maps and the location of errors in these models, *Acta Crystallogr. A47*, 110−119.
41. Brünger, A. T. (1992) Free *R* value: a novel statistical quantity for assessing the accuracy of crystal structures, *Nature 355*, 472−474.
42. Brünger, A. T., Adams, P. D., Clore, G. M., DeLano, W. L., Gros, P., Grosse-Kunstleve, R. W., Jiang, J. S., Kuszewski, J., Nilges, M., Pannu, N. S., Read, R. J., Rice, L. M., Simonson, T., and Warren, G. L. (1998) Crystallography & NMR system: a new software suite for macromolecular structure determination, *Acta Crystallogr. D54*, 905−921.
43. Brünger, A. T. (1988) Crystallographic refinement by simulated annealing: application to a 2.8 Å resolution structure of aspartate aminotransferase, *J. Mol. Biol. 203*, 803−816.
44. Brünger, A. T., Karplus, M., and Petsko, G. A. (1989) Crystallographic refinement by simulated annealing: application to a 1.5 Å resolution structure of crambin, *Acta Crystallogr. A45*, 50−61.
45. Laskowski, R. A., MacArthur, M. W., Moss, D. S., and Thornton, J. M. (1993) PROCHECK: a program to check the stereochemical quality of protein structures, *J. Appl. Crystallogr. 26*, 283−291.
46. Rossman, M. G., Liljas, A., Brändén, C. I., and Banasazak, L. J. (1975) Evolutionary and structural relationships among the dehydrogenases, in *The Enzymes* (Boyer, P. D., Ed.) 3rd ed., Vol. 11A, pp 61−102, Academic Press, New York.
47. Eisenhaber, F., and Argos, P. (1993) Improved Strategy in Analytic Surface Calculation for Molecular Systems: Handling of Singularities and Computational Efficiency, *J. Comput. Chem. 14*, 1272−1280.
48. Eisenhaber, F., Lijnzaad, P., Argos, P., Sander, C., and Scharf, M. (1995) The Double Cube Lattice Method: Efficient Approaches to Numerical Integration of Surface Area and Volume and to Dot Surface Contouring of Molecular Assemblies, *J. Comput. Chem. 16*, 273−284.
49. Glaser, L., and Zarkowsky, H. (1971) Dehydration in nucleotide-linked deoxysugar synthesis, in *The Enzymes* (Boyer, P. D., Ed.) 3rd ed., Vol. 5, pp 465−480, Academic Press, New York.
50. Bellamacina, C. R. (1996) The nicotinamide dinucleotide binding motif: a comparison of nucleotide binding proteins, *FASEB J. 10*, 1257−1269.
51. Swanson, B. A., and Frey, P. A. (1993) Identification of lysine 153 as a functionally important residue in UDP-galactose 4-epimerase from *Escherichia coli*, *Biochemistry 32*, 13231−13236.
52. Liu, Y., Vanhooke, J. L., and Frey, P. A. (1996) UDP-Galactose 4-Epimerase: NAD^+ Content and a Charge-Transfer Band Associated with the Substrate-Induced Conformational Transition, *Biochemistry 35*, 7615−7620.
53. Liu, Y., Thoden, J. B., Kim, J., Berger, E., Gulick, A. M., Ruzicks, F. J., Holden, H. M., and Frey, P. A. (1997) Mechanistic Roles of Tyrosine 149 and Serine 124 in UDP-galactose 4-Epimerase from *Escherichia coli*, *Biochemistry 36*, 10675−10684.
54. Thoden, J. B., Gulick, A. M., and Holden, H. M. (1997) Mechanistic roles of tyrosine 149 and serine 124 in UDP-galactose 4-epimerase from *Escherichia coli*, *Biochemistry 36*, 10675−10684.
55. Thoden, J. B., and Holden, H. M. (1998) Dramatic differences in the binding of UDP-galactose and UDP-glucose to UDP-galactose 4-epimerase from *Escherichia coli*, *Biochemistry 37*, 11469−11477.
56. Kessler, A. C., Brown, P. K., Romana, L. K., and Reeves, P. R. (1991) Molecular cloning and genetic characterization of the *rfb* region from *Yersinia pseudotuberculosis* serogroup IIA, which determines the formation of the 3,6-dideoxyhexose abequose, *J. Gen. Microbiol. 137*, 2689−2695.
57. Berman, H. M., Westbrook, J., Feng, Z., Gilliland, G., Bhat, T. N., Weissig, H., Shidyalov, I. N., and Bourne, P. E. (2000) The Protein Data Bank, *Nucleic Acids Res. 28*, 235−242.
58. Nelsestuen, G. L., and Kirkwood, S. (1971) The mechanism of action of the enzyme uridine diphosphoglucose 4-epimerase: proof of an oxidation−reduction mechanism with direct transfer of hydrogen between substrate and the B-position of the enzyme-bound pyridine nucleotide, *J. Biol. Chem. 246*, 7533.
59. Hallis, T. M., and Liu, H.-w. (1998) Stereospecificity of hydride transfer for the catalytically recycled NAD^+ in CDP-D-glucose 4,6-dehydratase, *Tetrahedron 54*, 15975−15982.
60. Byun, S. M., and Jenness, R. (1981) Stereospecificity of L-*myo*-inositol-1-phosphate synthase for nicotinamide adenine dinucleotide, *Biochemistry 20*, 5174−5177.
61. Jin, X., and Geiger, J. H. (2003) Structures of NAD^+ and NADH-bound 1-L-*myo*-inositol 1-phosphate synthase, *Acta Crystallogr. D59*, 1154−1164.
62. Bohren, K. M., Grimshaw, C. E., Lai, C. J., Harrison, D. H., Ringe, D., Petsko, G. A., and Gabbay, K. H. (1994) Tyrosine-48 is the proton donor and histidine-110 directs substrate stereochemical selectivity in the reduction reaction of human aldose reductase: enzyme kinetics and crystal structure of the Y48H mutant enzyme, *Biochemistry 33*, 2021−2032.
63. Thoden, J. B., Hegeman, A. D., Frey, P. A., and Holden, H. M. (1999) Molecular structure of dTDP-glucose 4,6-dehydratase from *Escherichia coli*, personal communication.
64. Kraulis, P. J. (1991) MOLSCRIPT: A Program to Produce Both Detailed and Schematic Plots of Protein Structures, *J. Appl. Crystallogr. 24*, 946−950.
65. Merritt, E. A., and Bacon, D. J. (1997) Raster3D: Photorealistic Molecular Graphics, in *Methods in Enzymology* (Carter, C. W., Jr., and Sweet, R. M., Eds.) Vol. 277, pp 505−524, Academic Press, New York.
66. Oppermann, U., Filling, C., Hult, M., Shafqat, N., Wu, X., Lindh, M., Shafqat, J., Nordling, E., Kallberg, Y., Persson, B., and Jornvall, H. (2003) Short-chain dehydrogenase/reductases (SDR): the 2002 update, *Chem.-Biol. Interact. 143−144*, 247−253.
67. Barton, G. J. (1993) ALSCRIPT: A tool to format multiple sequence alignments, *Protein Eng. 6*, 37−40.

BI035547F